



# Analysis of Corrosion Evolution in Carbon Steel in the Subtropical Atmospheric Environment of Sichuan

Chao Hai, Zhigao Wang, Fangyuan Lu, Shipeng Zhang, Cuiwei Du, Xuequn Cheng, and Xiaogang Li

Submitted: 18 August 2020 / Revised: 8 June 2021 / Accepted: 9 June 2021

As a part of Corrosion Map of Sichuan project, atmospheric corrosion behavior of carbon steel was investigated in the subtropical atmospheric environment by weight loss method at five exposure stations. Results indicated that an annual corrosion rate of carbon steel was between 0.66 and 23.6  $\mu\text{m}/\text{y}$ . The morphology and composition of corrosion products formed on the exposed steels were identified by scanning electron microscopy (SEM), energy-dispersive x-ray spectroscopy (EDS) and Raman spectroscopy. Subtropical atmospheric corrosion rate of the steel increases in high-rainfall and temperature environment. Bigger and deeper pits are preferred to form in a humid atmosphere. The corrosion products exhibited an uneven distribution and consisted mainly of goethite ( $\alpha\text{-FeOOH}$ ), lepidocrocite ( $\gamma\text{-FeOOH}$ ), magnetite ( $\text{Fe}_3\text{O}_4$ ) and hematite ( $\text{Fe}_2\text{O}_3$ ). The electrochemical corrosion of carbon steel in solution is an activation-controlled process, and a stable passive region was not observed for the steel. Electrochemical measurements showed that deposits on carbon steel decreased the corrosion resistance.

**Keywords** atmospheric corrosion, sichuan–tibet railway, carbon steel

## 1. Introduction

Atmospheric corrosion of structures proceeds via an electrochemical reaction with substances in the environment. The results of global studies have shown that corrosion costs amount to at least 4–5% of the GDP (Ref 1), with atmospheric corrosion as the major contribution to this cost. Previous researchers (Ref 2, 3) have correlated the corrosion rate of exposed metal with the climatic environment and pollution factors. It is generally believed that the main environmental factors that are considered to affect the atmospheric corrosion performance of materials are as follows (Ref 4-7): (1) the period over the temperature is above zero and the critical humidity (80%) is exceeded (the wetting time); (2) the  $\text{SO}_2$  content; and (3) the salt particles contents.

Due to widespread use of mild steel, it was considered desirable to study the corrosion behavior of these materials in a wide variety of atmosphere (Ref 7-10). Previous studies (Ref 11-13) have mostly been focused on the corrosion behavior of materials in environment of single or multiple key cities. Wang (Ref 14) et al. studied the atmospheric corrosion law of mild steel and weathering steel in tropical rain forest, marine atmosphere and industrial atmosphere. The results showed that the mild steel presented the highest corrosion rate in high humid and hot marine atmosphere. Cheng (Ref 11) et al.

studied the atmospheric corrosion of mild steel in Chongqing, China (industry polluted atmosphere environment). Yu (Ref 15) et al. studied the atmospheric corrosion behavior of Q235 and Q450W steel in Turpan, China (hot and dry environment). Furthermore, many research teams have studied the atmospheric corrosion behavior of various metal materials under different environmental conditions (Ref 17-23). Nevertheless, research has ignored the difference of corrosion behavior of materials across regions for a long time partly. Systematic and effective research has not been carried on the corrosion behavior of materials across different regions, especially in subtropical atmospheric environments. It is of considerable economic and social significance to correctly determine the corrosivity of an atmosphere, classify different regions based on differences in material corrosivity.

In the present study, carbon steel was exposed to 5 substations of subtropical atmospheric environment. The corrosion behaviors of Q235 carbon steel were investigated to lay a foundation for further analysis of the corrosion behaviors and mechanisms of carbon steel in the complex Subtropical atmospheric environment.

## 2. Experimental

### 2.1 Experimental Site Selection

The test stations were located in the main cities along Sichuan–Tibet railway. The corrosion of transmission equipment was investigated in this study.

The climate parameters of all the test stations were obtained from data released by the local climate bureau, including the average temperature, relative humidity and rainfall. The environmental pollutant contents (such as the  $\text{SO}_2$  and Cl ion concentrations) were determined by specific devices according to national standards. The experimental material was Q235 carbon steel and had the following main components (%): C: 0.16, Si: 0.20, Mn: 0.61,  $s < 0.023$ ,  $P < 0.019$ , Fe marginal. The atmospheric exposure samples were fabricated with

Chao Hai, Fangyuan Lu, Shipeng Zhang, Cuiwei Du, Xuequn Cheng, and Xiaogang Li, Institute of Advanced Materials and Technology, University of Science and Technology, Beijing, Beijing 100083, China; and Zhigao Wang, State Grid Sichuan Electric Power Research Institute, Chengdu 610041, China. Contact e-mail: dcw@ustb.edu.cn.

dimensions of 150 mm × 75 mm × 3 mm samples following the national standard. Firstly, the samples were turned and the original weight was weighted and recorded with an analytical balance with an accuracy of 0.0001 g.

The corrosion product covering the surface of the sample was removed using a solution of hydrochloric acid and hexamethylenetetramine (Ref 24). The corrosion rate,  $R$  ( $\mu\text{m}/\text{y}$ ), was calculated by the following equation:

$$R = \frac{(w_0 - w_t) \times 10^4}{S\rho t} \quad (\text{Eq 1})$$

where  $R$  represents the corrosion weight loss rate,  $\mu\text{m}/\text{a}$ ;  $W_0$  represents the original weight of the sample, g;  $W_t$  represents the sample weight after removal of the corrosion product, g;  $S$  represents the exposed area of the sample,  $\text{cm}^2$ .  $P$  represents the density of Q235 carbon steel,  $7.86\text{g}/\text{cm}^3$ ; and  $t$  represents the exposure time of the sample to the atmosphere, years, where  $t = 1\text{a}$ .

## 2.2 Corrosion Morphology Observation

The surface and cross-sectional morphologies of the rust layer on the carbon steel samples were observed by a Quanta 250 SEM. The chemical compositions of the corrosion products and the elemental distribution on the cross section of a product film were analyzed by EDS.

The corrosion products of samples exposed for 1 year were analyzed by Raman spectroscopy. The laser wavelength of the Raman spectrometer was 532 nm, the laser intensity was set to 5%, the exposure time was 10s, and the Raman displacement measurement range was  $0 \sim 1800 \text{ cm}^{-1}$ .

A rust removal solution was selected to clean the corrosion products off the sample surface following GB/T 19746-2005. The components of the rust remover were 500 ml hydrochloric acid + 500 ml deionized water + 3.5 g hexamethylenetetramine. After being cleaned and dried, the samples were observed under a Keyence VHX-2000 3D laser confocal microscope to obtain precise morphological parameters, such as the pit depth.

## 2.3 Electrochemical Test

The electrochemical measurements were taken by a 3F electrochemical workstation in a 3.5% NaCl solution with a three-electrode system, using a Pt plate as the counter electrode and a saturated calomel electrode (SCE) as the reference electrode. On-site corrosion tests were performed after one year of sample exposure using Q235 carbon steel as the working electrode. Each steel sample was cut into a  $10 \text{ mm} \times 10 \text{ mm} \times 4 \text{ mm}$  piece and covered with epoxy resin, leaving an exposed area of  $1 \text{ cm}^2$ . The scan rate of the polarization curve was  $0.5 \text{ mV}/\text{s}$ , the electrochemical impedance test frequency was  $10 \text{ mHz} \sim 100 \text{ kHz}$ , and the amplitude was 10 mV. The system was allowed to stabilize for 60 min at a solution temperature of  $25 \text{ }^\circ\text{C}$  before conducting the electrochemical test.

# 3. Results

## 3.1 Environmental and Corrosive Characteristics of Test Station

Table 1 displays the environmental conditions at the exposure stations. The average temperature and rainfall at all

the stations show significant seasonal variation. The highest rainfall generally occurred in June, July and August. Meanwhile, in the months with heavy rainfall, the temperature is relatively high, showing the characteristics of rainy and hot seasons. Table 2 shows the environment pollutant content for the five exposure stations. The  $\text{SO}_2$  pollutant level and Cl deposition rate level were considered to be fairly low relative to the national standard (Ref 27).

Figure 1 shows the corrosion rates of Q235 carbon steel under atmospheric exposure in five areas. The highest corrosion rate among the five Q235 carbon steel samples after 1 year of exposure was obtained for the Yaan sample, whereas the corrosion rates of the Batang and Litang samples were relatively low. Note that the corrosion of carbon steel in the subtropical atmospheric environment was not significant compared with marine atmospheres (Ref 7, 17, 28) and acidic atmospheres (Ref 8, 19), which are considered to contain a large quantity of pollutants, such as  $\text{SO}_2$ . The corrosion grades for the five areas were determined based on the corrosion rate of carbon steel. According to the GB/T 19292.1-2003/ISO 9223:1992, corrosion grade C1 represents  $R \leq 1.3\mu\text{m}/\text{y}$  and C2 represents  $1.3 < R \leq 25 \mu\text{m}/\text{y}$ . Thus, the atmospheric corrosion level is C2 for the Chengdu, Yaan, and Kangding areas and C1 for the Litang and Batang areas.

## 3.2 Corrosion Morphology and EDS Analysis

The surface morphologies of the corrosion product formed on Q235 steel are shown in Figure 2. The images show comparatively compact and flat rust layers formed on Q235 steel at the Chengdu, Yaan and Kangding stations. Many cracks exist in the corroded steel sample from the Litang station, whereas only a few spherical-shaped products appear on the surface of the Batang station sample. Figure 2 shows the details surface morphologies observed at high magnification. Root-shaped globular substances can be observed at positions A (see Fig. 3a) and C (see Fig. 2c), although the particle are smaller at position C than at position A. the corrosion product at position B (see Fig. 2b) is comparatively flatter with few bulges. A plate with a few large cracks can be observed at Position D. By contrast, plenty of spherical products are abundant on the surface at position E, as be clearly observed in the locally enlarged image. Figure 2 shows the EDS results for the corrosion products on steel after 1 year of atmospheric exposure, where the main elements are Fe, O, Al and Si. More detailed analysis is given in the following part.

The cross-sectional morphologies of the corrosion product formed on Q235 steel were observed by SEM, and the map distributions of O, Fe and Si or Al were determined by EDX, as shown in Figure 3. A continuous layer of rust formed on the surfaces of samples exposure at Chengdu, Yaan and Kangding stations for a year. The product films contain many clearly observable cracks, some of which occur near the matrix, as marked by the yellow arrows. Cracks facilitate the passage of the corrosive medium through the rust layer to contact the matrix, thus increasing matrix corrosion.

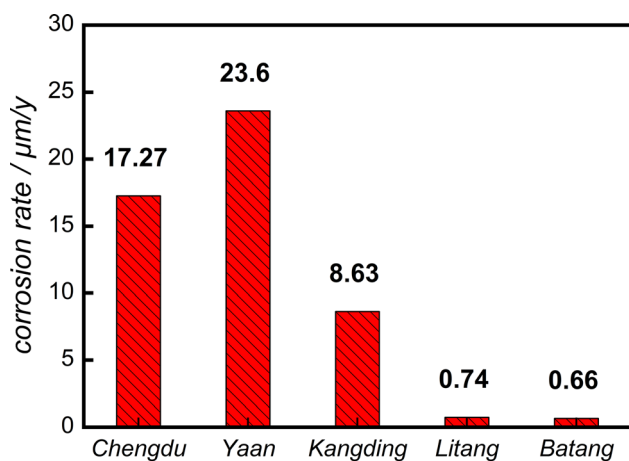
The rust layer thickness is shown in Figure 4. Note that the variation trend in the rust layer thickness is consistent with that for the corrosion rate of carbon steel shown in Fig. 1 and 4. That is to say, the sample from the Yaan area has the largest corrosion rate, where the corresponding rust layer thickness reaches  $56.34 \mu\text{m}$ . This result was obtained because the loose porous rust layer product in high-rainfall environment does not

**Table 1 Environmental conditions at the test exposure stations**

Exposure station		Meteorological data (2017.01–2018.01)											
1	2	3	4	5	6	7	8	9	10	11	12		
1	Average temperature/ °C	7.3	8.2	11.1	17.2	21.5	23.4	26.7	25.9	22.3	16.5	12.4	6.5
	Average relative humidity/%	81	81	81	76	71	80	81	85	86	90	83	80
	Average rainfall /mm	4.3	20.5	33.9	57.9	33.7	72.1	383.3	249.0	38.6	61.5	10.7	1.4
2	Average temperature (°C)	8.3	8.8	11.5	17.5	21.5	23.4	27.4	26.1	22.1	16.4	13.2	8.6
	Average relative humidity/%	80	80	81	76	69	76	70	81	83	91	83	74
	Average rainfall /mm	19.4	25.3	77.0	103.1	114.0	116.0	184.8	575.0	107.7	120.6	19.5	11.3
3	Average temperature/°C	/	1.3	2.7	8.3	11.3	13.1	16.6	16.9	13.5	9.0	3.9	−0.1
	Average relative humidity/%	70	71	82	78	80	86	78	86	91	91	81	77
	Average rainfall /mm	/	25.1	36.5	120.5	161.9	225.6	92.7	119.9	112.6	82.4	17.3	0.4
4	Average temperature/°C	−5.2	−1.9	0.7	4.5	8.9	10.5	11.3	12.8	9.6	7.6	2.5	−1.2
	Average relative humidity/%												
	Average rainfall /mm	0.2	24.6	8.6	47.8	33.4	166.9	243.7	72.3	160.9	3.7	2.5	3.6
5	Average temperature/°C	4.3	8.8	11.4	13.8	17.8	19.2	19.5	20.9	16.2	14.9	9.6	5.4
	Average relative humidity/%												
	Average rainfall /mm	/	9.3	1.1	30.2	50.6	165.6	167.5	43.4	138.9	6.6	/	/

**Table 2 Average sulfur dioxide and chloride deposition rate and atmospheric classification categories**

Exposure station		SO <sub>2</sub>		Cl <sup>-</sup>		NO <sub>2</sub>
No.	Location	Concentration, µg m <sup>-3</sup>	classification	Deposition rate, mg/m <sup>2</sup> /d	classification	Average concentration, µg m <sup>-3</sup>
1	Chengdu	9.4	P0	0.37	S0	48.1
2	Yaan	14.5	P0	0.09	S0	20.8
3	Kangding	10.4	P0	0.10	S0	15.9
4	Litang	7.8	P0	0.11	S0	9.7
5	Batang	/	/	/	/	12.6

**Fig. 1** Corrosion rates of Q235 steels after exposure for 1 year

provide adequate protection for the sample which contains a large number of microcracks and cavities. The product films facilitate the passage of the corrosive medium and thereby the development of the corrosion reaction to increase the quantity of corrosion. High corrosion can occur during short periods and lead to failure or fracture of metallic materials. The properties of rust layers will be discussed in the following section. Note that relatively low sample corrosion occurs in Litang and Batang environments. Corrosion occurs at isolated points on the sample surface, and a continuous rust layer does not form.

Thus, the data for these two areas are not included in the section analysis and thickness statistics.

### 3.3 Phase Analysis of Corrosion Products

The compositions of the corrosion products were investigated by Raman spectroscopy, as shown in Fig. 5. Table 3 shows the main Raman bands of the reference iron oxide compounds. Similar major phases of the rust layer are obtained for the sample, and the main Raman peaks of the product films appear at 217, 287, 387, 480, 666 and 1304 cm<sup>-1</sup>. According to Table 1, the Raman spectra are determined to be composed of goethite ( $\alpha$ -FeOOH), lepidocrocite ( $\gamma$ -FeOOH) and magnetite (Fe<sub>3</sub>O<sub>4</sub>), as determined from the Raman spectra and published papers (Ref 25, 26). The peak at 248 cm<sup>-1</sup> in the Raman curve of the rust layer for Litang and Batang sample corresponds to  $\alpha$ -Fe<sub>2</sub>O<sub>3</sub>. Previous studies have indicated the existence of  $\alpha$ -Fe<sub>2</sub>O<sub>3</sub> in rust layers, which mostly forms in the early stage of corrosion under low temperature (Ref 29). Therefore, corrosion of carbon steel develops slowly in low-temperature areas, where a portion of the products are generated during the early stage of corrosion.

Figure 6 presents the corrosion morphologies of the Q235 steel samples after rust removal. Quite different corrosion morphologies can be observed for carbon steel samples exposed in different areas. The Yaan exposure station area clearly produces the most severe corrosion, with a large pit size and depth. These pits are wide in the horizontal direction, with widths of up to 500 µm and depth of 95 µm. A comparison of

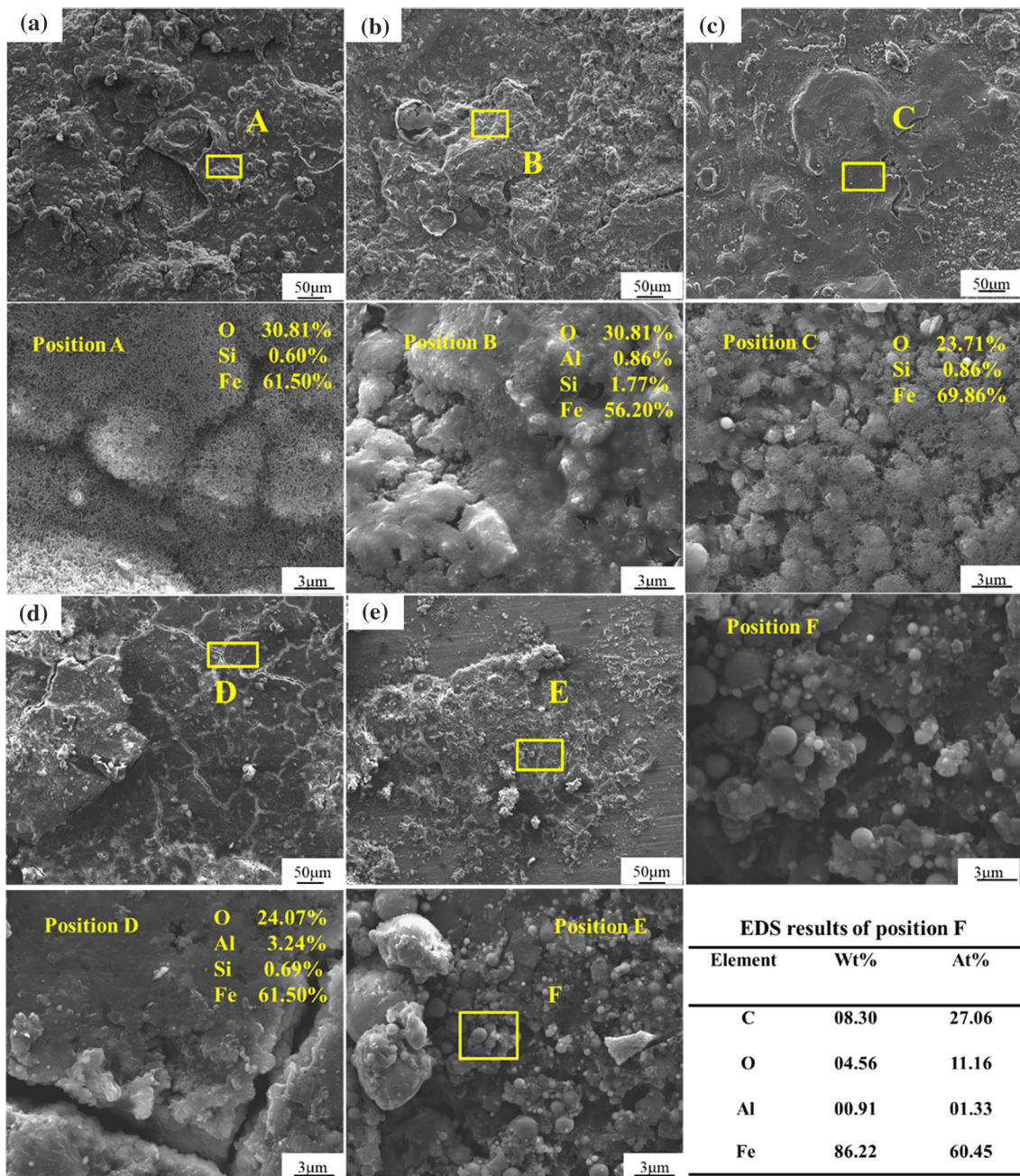


**Fig. 2** Surface morphologies of Q235steels after 1 year of exposure at five stations for 1 year(a) Chengdu, (b) Yaan, (c) Kangding, (d) Litang, (e) Batang

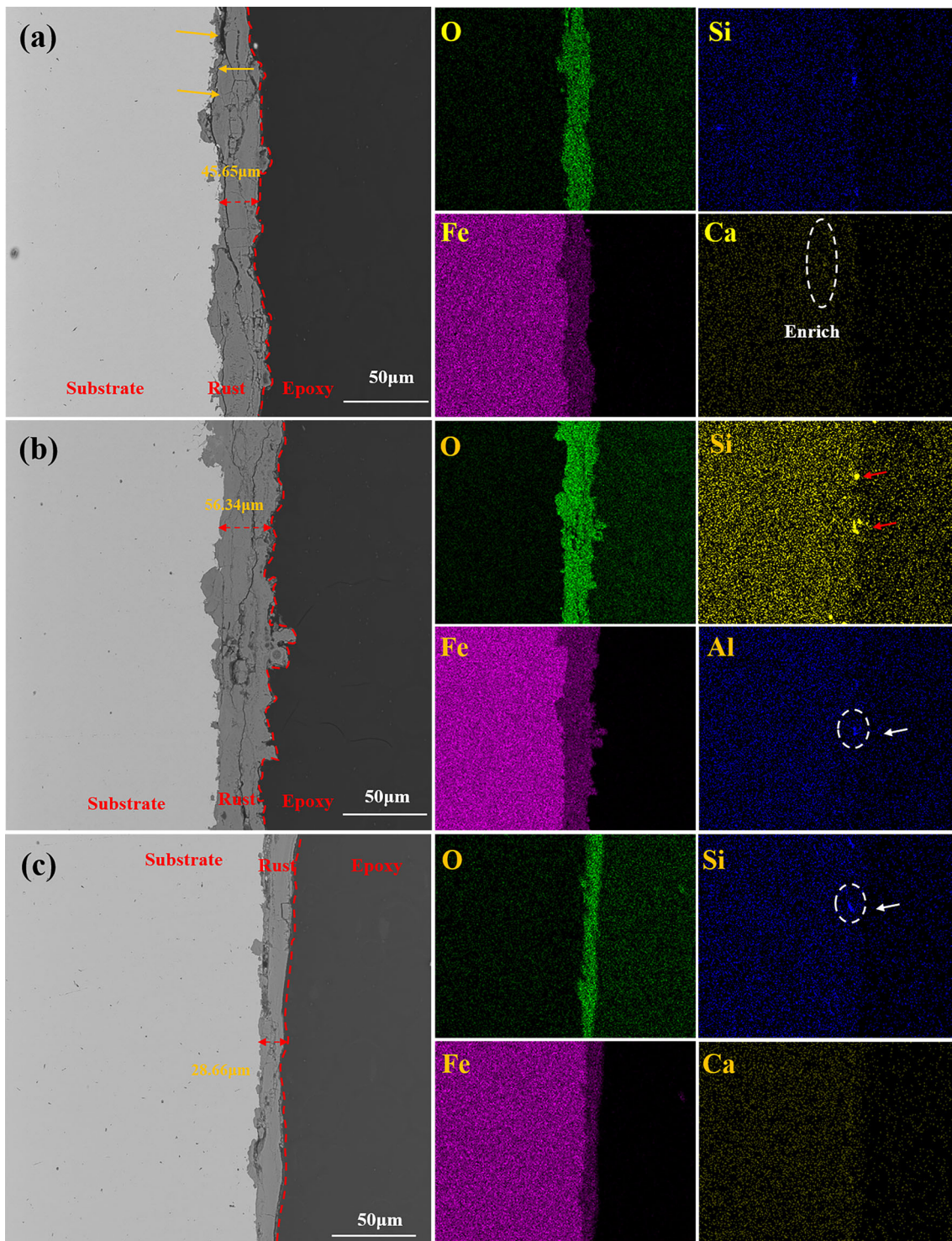
Fig. 6(a) and (c) shows deeper pits for the Chengdu sample than for the Kangding sample. Figure 6 (d) and (e) shows few pits on the sample surfaces, with clearly visible processing traces for most areas.

Figure 7 shows the results of a detailed statistical analysis of the pits of the samples after rust removal. The average pit depths of the exposed carbon steel were 41.6, 48.5, 30.6, 9.8 and 9.1  $\mu\text{m}$ . The area ratios of the corrosion pits were determined to be 33.658, 39.259, 28.347, 9.012 and 8.365%. Thus, the Yaan sample contains deeper and larger pits than those from other areas because of the relatively higher rainfall and temperature of the Yaan area.

### 3.4 Electrochemical of the Rust Layers

The structure and composition of the product films on Q235 carbon steel exposed at the five stations were investigated. Polarization and EIS measurements were taken to evaluate the properties of the product films.

Figure 8 shows the polarization curves of the carbon steel after a year of exposure at the five exposure stations. The electrochemical corrosion of carbon steel is an activation-controlled process, and a stable passive region was not observed for the steel. The curves clearly exhibit two regimes. The corrosion current densities ( $I_{\text{corr}}$ ) and the corrosion potentials ( $E_{\text{corr}}$ ) of carbon steel were evaluated, and fitting



**Fig. 3** Cross-sectional morphologies of the product film form on (a) Chengdu, (b) Yaan and (c) Kangding

results are shown in Table 4. The fitting results show a high current density for the Chengdu, Yaan and Kangding samples than that Litang and Batang samples. The results indicate that the product films formed on Chengdu, Yaan and Kangding samples are susceptible to corrosion in salt solution and do not provide effective resistance to the passage of the corrosive medium. The Litang and Batang samples exhibit low corrosion

of carbon steel and therefore have similar electrochemical properties to bare steel, with low corrosion current densities and corrosion potentials.

Figure 9 presents the EIS of carbon steel after 1-year exposure at the five stations. The curves for the Batang and Litang samples clearly exhibit a single capacitive reactance, where the radius of the capacitance arc is large for the Litang

sample than for the Batang sample. The curves of the samples from Chengdu, Yaan and Kanding exhibit capacitance and diffusion resistance arcs. Combined with the Bode-phase

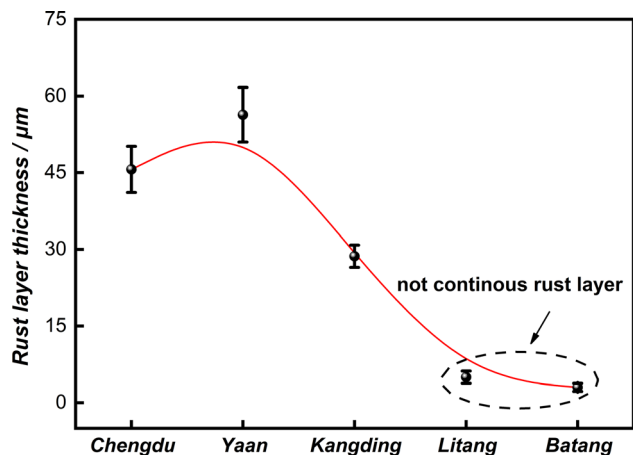


Fig. 4 The thickness of rust layer of Q235 steel after 1 year of exposure at five stations

diagram, it can be found that the corroded specimens appear one time constant at the low-frequency band, which implies that one state variable affects the electrochemical reaction process of Q235 steel. However, as for the EIS results from Chengdu, Yaan and Kanding, an additional state variable shows up and plays a role during the electrode reaction, which can be attributed to the different structures of the corrosion product films.

Based on the above analysis, the EIS curves can be simulated using appropriate equivalent electric circuits.  $R(QR)$  was used for Litang and Batang samples data, whereas  $R(Q(R(Q(RW))))$  was used for the Chengdu, Yaan and Kanding sample data, as shown in Fig. 10. The effects of inhomogeneity, porosity, mass transport and relaxation of the electrode result in deviation from ideal capacitance characteristics. Therefore, the constant phase angle element  $Q$  should replace the pure capacitance  $C$  in fitting EIS spectrum to simulate the dispersion characteristics, where the following definitions are used:  $R_s$  is the solution resistance;  $Q_1$  and  $R_r$  are the capacitance and resistance of the product film, respectively;  $R_{ct}$  is the charge transfer resistance;  $Q_{dl}$  represents the capacitance of the double electrode layer; and  $W$  is the Warburg impedance.

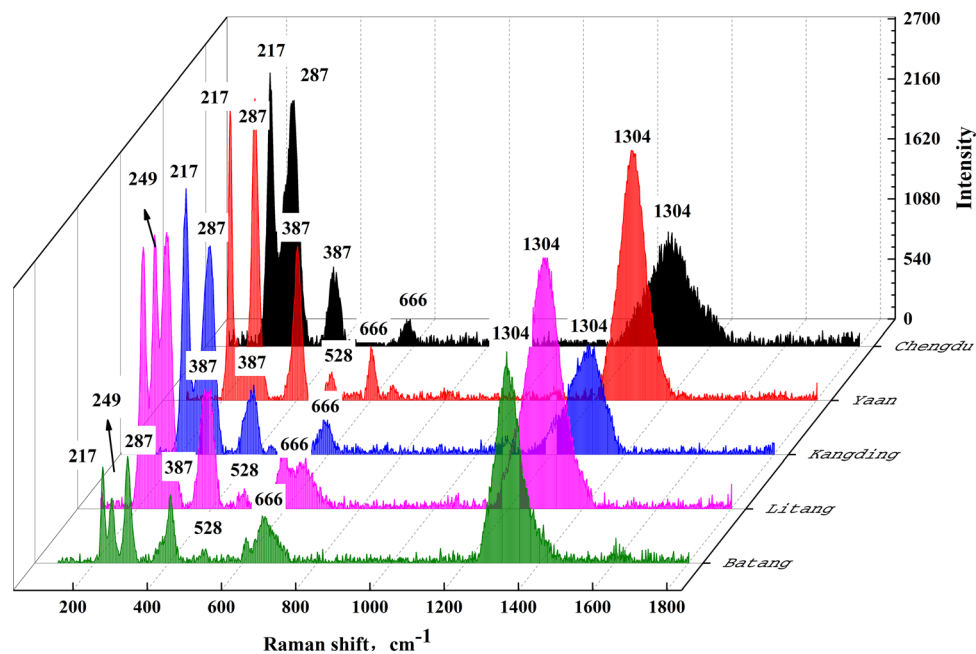
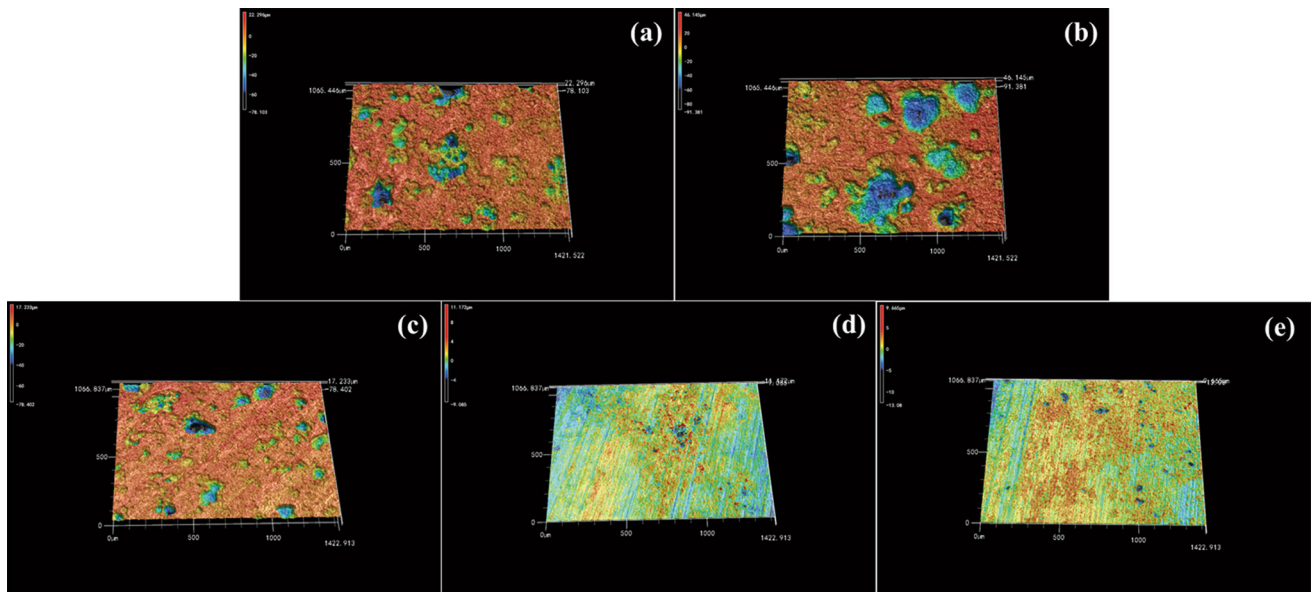


Fig. 5 Raman spectra results of the corrosion product formed on Q235steels after 1 year of exposure at five stations

Table 3 Main Raman bands of reference iron oxide compounds (Ref 25, 26)

Phase	Peak and shoulders observed on the reference spectra
Goethite ( $\alpha$ -FeOOH)	203, 244, 300, <u>387</u> , 399, 415, 480, 552, 684, 1002, 1113, 1304
Akaganéite ( $\beta$ -FeOOH)	139, 308, 331, 389, 420, 499, 539, 609, 720, 1410
Lepidocrocite ( $\gamma$ -FeOOH)	166, <u>217</u> , <u>251</u> , 310, 350, 378, 529, 655, 713, 1300
Hematite ( $Fe_2O_3$ )	<u>228</u> , 250, 294, 414, 502, 625, 670, 1330
Magnetite ( $Fe_3O_4$ )	306, 538, <u>666</u>
Maghemite ( $\gamma$ - $Fe_2O_3$ )	339–386, 461–512, 671–717, 1430
Hematite ( $\alpha$ - $Fe_2O_3$ )	227, 245, <u>293</u> , <u>298</u> , <u>414</u> , 501, 612

Note: The strongest peak for each compound is underlined.



**Fig. 6** 3D surface morphology of Q235 steels after 1 year of exposure at five stations. (a) Chengdu, (b) Yaan, (c) Kangding, (d) Litang and (e) Batang

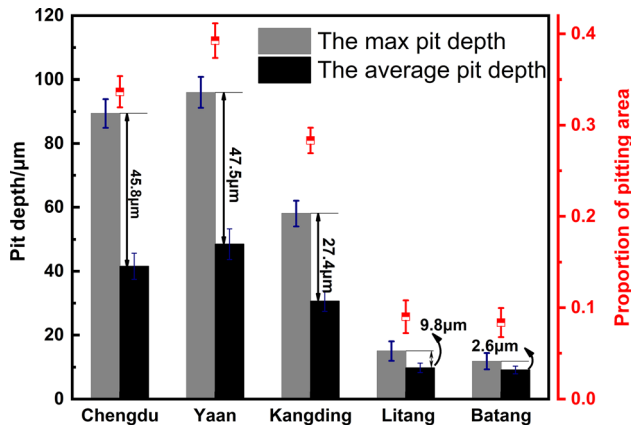


**Fig. 7** Depth and proportion of pit area of Q235 steels after 1 year of exposure at five exposure stations

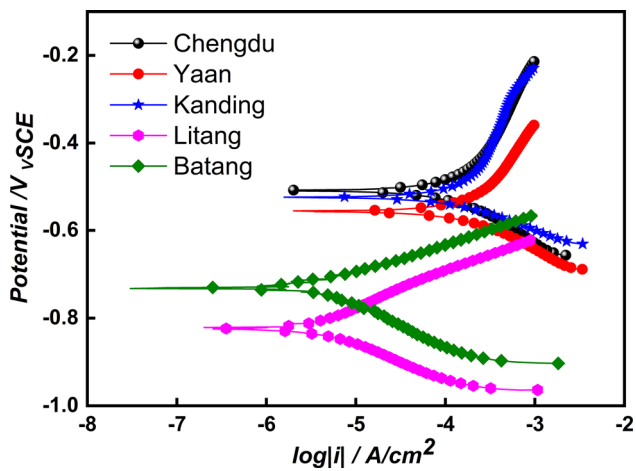


**Fig. 8** Potentiodynamic polarization curve of Q235 steels after 1 year of exposure at five stations in 3.5% NaCl solutions

**Table 4** Polarization curve fitting data for Q235 steel exposed to the atmosphere

No.	Exposure Location	Parameter			
		E (mv)	$I_{corr}$ ( $\mu\text{A}\cdot\text{cm}^{-2}$ )	$\beta_a$	$\beta_c$
1	Chengdu	-510.9	81.4	146.63	88.13
2	Yaan	-551.3	104.2	103.35	89.52
3	Kangding	-522.1	87.8	121.65	67.73
4	Litang	-822.6	3.5	93.145	78.5
5	Batang	-726.9	2.7	63.18	71.29

Table 5 shows the changes in the  $R_{ct}$  and  $R_r$  of the samples with product films exposed at the five stations. In Chengdu, Yaan and Kangding stations,  $R_r$  of the rust layer is larger. An opposite trend is observed for the change of  $R_{ct}$  of the exposed samples. The larger  $R_{ct}$  is, the more difficult charge transfer. The small  $R_{ct}$  for severely corrosion environments indicates a significant decrease in the difficulty of charge transfer during corrosion.

#### 4. Discussions

Under the complexity of atmospheric environments, the corrosion behavior of carbon steels should be carefully considered. Based on the results above, the corrosion law of Q235 steel in the same area is basically similar, but the corrosion kinetics process is quite different. A comparison of the corrosion results and environmental data (Figure 2 and Table 2) shows the complex influence of environmental parameters on atmospheric corrosion. Increase in rainfall and humidity can promote the corrosion of carbon steel (Ref 8, 12), whereas low temperatures inhibit the electrochemical process of corrosion (Ref 29). This can be explained as follows. Loose rust layers with many cavities and cracks were formed on the

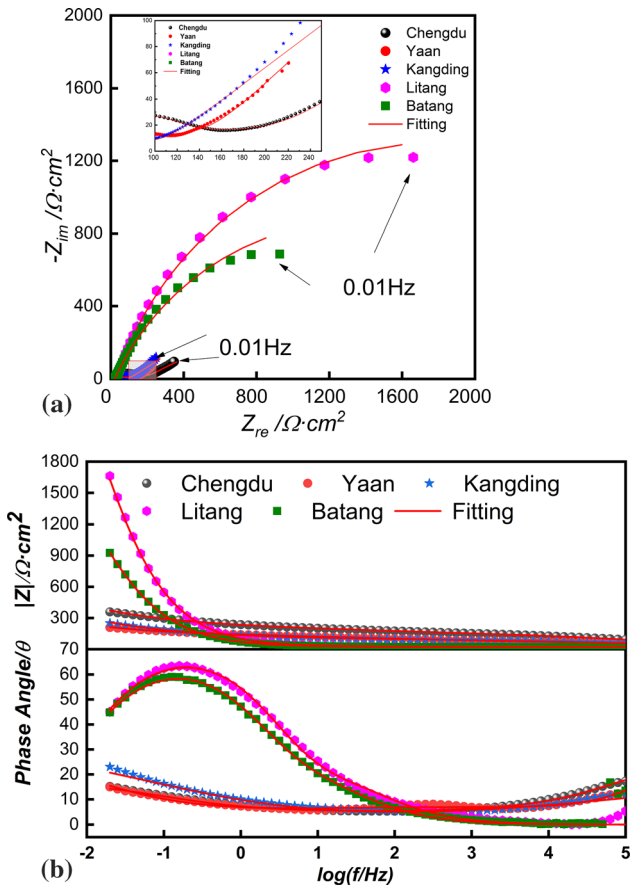


**Fig. 9** EIS results for Q235 steels after 1 year of exposure at five stations in 3.5% NaCl solutions: (a) Nyquist; (b) Bode

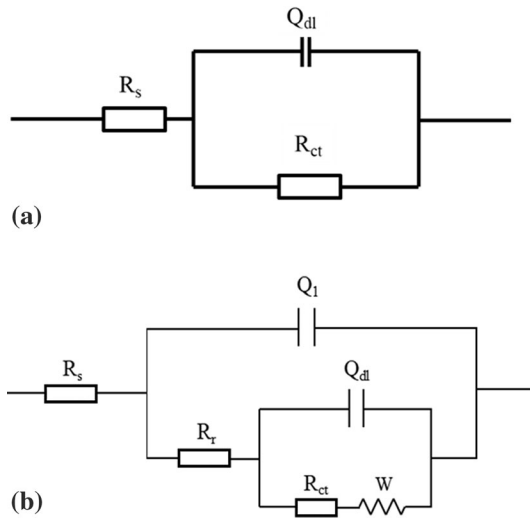
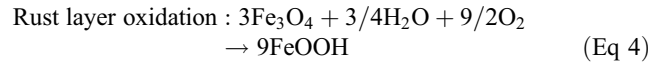
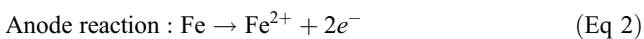
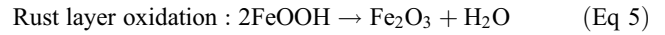


**Fig. 10** Equivalent EIS electrochemical circuit

surface of carbon steel in humid environments, which the oxygen and water can easily penetrate. An abundance of oxygen and water in the rust layer promotes the reactions process. The corresponding chemical reactions are as follows (Ref 7, 8, 23, 31):



FeOOH is unstable and transforms to Fe<sub>2</sub>O<sub>3</sub>·H<sub>2</sub>O, for which there are several varieties, the most common varieties being goethite (α-FeOOH) and γ-form of lepidocrocite (γ-FeOOH) that is produced by reaction with oxygen (Ref 32). The final product is the familiar rust Hematite from lepidocrocite.



Based on the previous studies (Ref 11, 13, 14), air pollutants in atmospheric environment, such as SO<sub>2</sub>, can promote the recycling process of H<sub>2</sub>SO<sub>4</sub> in rust layer. Thus, the acid recycling mechanism can accelerate the anodic activation dissolution and cathodic hydrogen evolution reaction at the same time, greatly promote the local corrosion of the metal matrix at the bottom of the rust layer and significantly improve the corrosion electrochemical process of carbon steel. According to Table 2, the content of air pollutants is less, which decreases the corrosion process of carbon steel for the lack of corrosive medium in the liquid film.

The atmospheric corrosion behavior of carbon steel at five areas in subtropical atmospheric environment is different. The corrosion rate of carbon steel in areas with low temperatures is about 1/35 of the highest corrosion rate. Therefore, as for structure materials, protective measures should be tailored to the corrosion rate of carbon steel in different environments, which has considerable economic repercussions. Note that the corrosion performance of carbon steel was investigated in this study, and few studies have been conducted on the mechanical properties of exposed carbon steel. The results presented in this paper show the development of deep pitting, especially in humid environments, where large pits increase the fracture sensitivity and reduce the service life of a material.

## 5. Conclusions

1. Corrosion rate of the steel increases in high rainfall and temperature environment. Bigger and deeper pits are preferred to form in a humid atmosphere.
2. Subtropical atmospheric The corrosion products of carbon steel exposed in different areas are mainly composed of the following phases: α-FeOOH, γ-FeOOH and Fe<sub>3</sub>O<sub>4</sub>. Fe<sub>2</sub>O<sub>3</sub> also exist in the rust layer. The deposit layer is not effective in reducing oxygen diffusion due to its loose, porous structure.
3. The electrochemical corrosion of carbon steel in solution is an activation-controlled process, and a stable passive region was not observed for the steel. The electrochemical results indicate a higher current density for samples exposed in areas with high temperature and rainfall.

**Table 5 EIS fitting data of Q235 steels after 1 year of exposure at five stations**

Exposure Location	Parameter								
	$R_s \Omega\text{-cm}^2$	$Q_1 \times 10^{-4} \Omega^{-1} \text{cm}^{-2} \text{s}^n$	$n_1$	$R_r \Omega\text{-cm}^2$	$Q_{dl} \times 10^{-4} \Omega^{-1} \text{cm}^{-2} \text{s}^n$	$n_{dl}$	$R_{ct} \Omega\text{-cm}^2$	$W \Omega\text{-cm}^2$	$\chi^2 \times 10^{-4}$
Chengdu	5.23	4.73	0.42	151	1.5	0.28	272	0.031	1.31
Yaan	8.32	5.34	0.45	103.75	2.3	0.34	102.2	0.042	3.21
Kangding	8.90	4.32	0.24	92.98	1.2	0.37	289.5	0.034	4.82
Litang	7.68	79.3	0.75	/	/	/	3505	/	1.26
Batang	4.23	41.9	0.73	/	/	/	2097	/	1.03

### Acknowledgments

This work was jointly supported by the Fundamental Research Funds for the Central Universities (No. FRF-MP-18-002) and the Science and Technology Project of State Grid Sichuan Electric Power Corporation of China (No. 521997160013).

### Conflict of interest

The authors declare no conflicts of interest.

### References

- S. Feliu and M. Morcillo, The Prediction of Atmospheric Corrosion from Meteorological and Pollution Parameters—i. Annual Corrosion, *Corros. Sci.*, 1993, **34**, p 403–414.
- S. Feliu and M. Morcillo, The Prediction of Atmospheric Corrosion from Meteorological and Pollution Parameters—ii. Long-term Forecasts, *Corros. Sci.*, 1993, **34**, p 415–422.
- C.F. Liang and W.T. Hou, Atmospheric Corrosivity for Steels, *J. Chin. Soc. Corros. Prot.*, 1998, **18**, p 1–6.
- F. Corvo, J. Minotas, J. Delgado and C. Arroyave, Changes in Atmospheric Corrosion Rate Caused by Chloride Ions Depending on Rain Regime, *Corros. Sci.*, 2005, **47**, p 883–892.
- M. Morcillo, S. Feliu and S. Giménez, Long-term Atmospheric Corrosion of Mild Steel, Zinc, Copper and Aluminium in Spain, *Key. Eng. Mater.*, 1991, **20–28**, p 17–26.
- M. Morcillo, S. Feliu and J. Simancas, Deviation from Bilogarithmic Law for Atmospheric Corrosion of Steel, *Br. Corros. J.*, 2013, **28**, p 50–52.
- P. Cui, N.S. Chen, Q. Zou, F.H. Su and Y.L. Zhang, Risk Assessment and Disaster Reduction Strategies for Mountainous and Meteorological Hazards in Tibetan Plateau, *Sci. Bull.*, 2015, **60**, p 3067–3077.
- Z. Song, G.Z. Zhang and L.W. Jiang, Engineering Geological Features and Geological Route Selection Principle of Sichuan-tibet Railway, *Rail. Eng.*, 2017, **000**, p 142–145.
- D. Wang, G.Z. Zhang, L.W. Jiang and J. Ouyang, Engineering Effect of Active Fault and Geological Alignment of Chengdu to Kangding in Sichuan-Tibet Railway, *J. Rail. Eng. Soc.*, 2015, **000**, p 6–11.
- X.S. Xia, S.Y. Dai, X.C. Chen and J.Z. Li, Seismic Design Criterion for Long-span Bridges of Sichuan-Tibet Railway, *J. Chin. Rail. Soc.*, 2016, **38**, p 85–89.
- X.Q. Cheng, Y.W. Tian, X.G. Li and C. Zhou, Corrosion Behavior of Nickel-Containing Weathering Steel in Simulated Marine Atmospheric Environment, *Mater. Corros.*, 2014, **65**, p 1033–1037.
- M. Natesan, G. Venkatachari and N. Palaniswamy, Kinetics of Atmospheric Corrosion of Mild Steel, Zinc, Galvanized Iron and Aluminium at 10 Exposure Stations in India, *Corros. Sci.*, 2006, **48**, p 3584–3608.
- W. Wu, X.Q. Cheng, H. Hou, B. Liu and X.G. Li, Insight into the Product Film Formed on Ni-advanced Weathering Steel in a Tropical Marine Atmosphere, *Appl. Surf. Sci.*, 2018, **436**, p 80–89.
- C. Wang, G.W. Cao, C. Pan, Z.R. Wang and M.R. Miao, Atmospheric Corrosion of Carbon Steel and Weathering Steel in Three Environments, *J. Chin. Soc. Corros. Prot.*, 2016, **36**, p 39–46.
- Q. Yu, C.F. Dong, Y.H. Fang, K. Xiao, C.Y. Guo, G. He and X.G. Li, Atmospheric Corrosion of q235 Carbon Steel and q450 Weathering Steel in Turpan, China, *J. Iron. Steel. Res. Int.*, 2016, **23**, p 1061–1070.

- X.C. Hao, X.G. Li, K. Xiao and C.F. Dong, Corrosion Behaviors at the Initial Stage of q235 Steel in Xisha Atmosphere, *J. Chin. Soc. Corros. Prot.*, 2009, **29**, p 465–470.
- S. Oesch and P. Heimgariner, Environmental Effects on Metallic Materials - Results of an Outdoor Exposure Programme Running in Switzerland, *Mater. Corros.*, 1996, **47**, p 425–438.
- P.S. Mohan, M. Natesan, M. Sundaram and K. Balakrishnan, Atmospheric Corrosion at Different Locations in South India, *Bull. Electrochem.*, 1996, **12**, p 91–92.
- Z.Y. Cui, X.G. Li, C. Man, K. Xiao, C.F. Dong, X. Wang and Z.Y. Liu, Exfoliation Corrosion Behavior of 2B06 Aluminum Alloy in a Tropical Marine Atmosphere, *J. Mater. Eng. Perform.*, 2015, **24**, p 296–306.
- D.C. Kong, C.F. Dong, Y.H. Fang, K. Xiao, C.Y. Guo, G. He and X.G. Li, Copper Corrosion in Hot and Dry Atmosphere Environment in Turpan, China, *Trans. Nonferrous. Met. Soc. China.*, 2016, **26**, p 1721–1728.
- Z.Y. Cui, K. Xiao, C.F. Dong, T.Y. Cui and X.G. Li, Long-term Corrosion Behavior of AZ31 Magnesium Alloy in Xisha Marine Atmosphere, *J. Univ. Sci. Technol.*, 2014, **36**, p 339–344.
- X.Q. Cheng, Z. Jin, M. Liu and X.G. Li, Optimizing the Nickel Content in Weathering Steels to Enhance their Corrosion Resistance in Acidic Atmospheres, *Corros. Sci.*, 2017, **115**, p 135–142.
- Q. Hou, Z.Y. Liu, C.T. Li and X.G. Li, Degradation of the Oxide Film Formed on Alloy 690TT in a High-temperature Chloride Solution, *Appl. Surf. Sci.*, 2019, **467–468**, p 1104–1112.
- GB/T 16545-2015 Chinese National Standard for Corrosion of Metals and Alloys — Removal of Corrosion Products from Corrosion Test Specimens, China State Bureau of Technical Supervision, Beijing, China, (2015)
- A. Demoulin, C. Trigance and D. Neff, The Evolution of the Corrosion of Iron in Hydraulic Binders Analysed from 46- and 260-Year-Old Buildings, *Corros. Sci.*, 2010, **52**, p 3168–3179.
- L.J. Oblonsky and T.M. Devine, Corrosion of Carbon Steels in CO<sub>2</sub>-Saturated Brine, *J. Electrochem. Soc.*, 1997, **144**, p 1252–1260.
- GB/T 19292.1-2003 Chinese National Standard for Corrosion of Metals and Alloys — Corrosivity of atmospheres-Classification, China State Bureau of Technical Supervision, Beijing, China, (2003)
- S.J. Oh, D.C. Cook and H.E. Townsend, Atmospheric Corrosion of Different Steels in Marine, Rural and Industrial Environments, *Corros. Sci.*, 1999, **41**, p 1687–1702.
- F.P. Fehlner and N.F. Mott, Low-temperature Oxidation, *Oxidation. Met.*, 1970, **2**, p 59–99.
- H. Antony, S. Perrin, P. Dillmann, L. Legrand and A. Chausse, Electrochemical Study of Indoor Atmospheric Corrosion Layers Formed on Ancient Iron Artefacts, *Electrochim. Acta*, 2007, **52**, p 7754–7759.
- D.C. Kong, C.F. Dong, X.Q. Ni and X.G. Li, Corrosion of Metallic Materials Fabricated by Selective Laser Melting, *Npj Material Degradation*, 2019, **3**, p p1-14.
- K. Xiao, C.F. Dong, X.G. Li and F.M. Wang, Corrosion Products and Formation Mechanism during Initial Stage of Atmospheric Corrosion of Carbon Steel, *J. Iron Steel Res. Int.*, 2008, **15**, p p42-48.

**Publisher's Note** Springer Nature remains neutral with regard to jurisdictional claims in published maps and institutional affiliations.